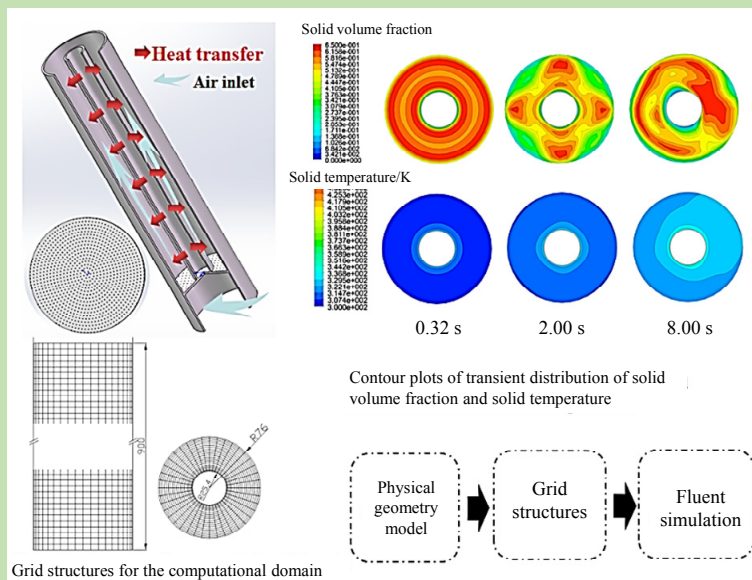


Numerical simulation on heat transfer in a cylindrical fluidized bed

Lijun WANG*, Shuping DUAN, Lingfeng XU, Jiajun SUN

College of Energy and Environment, Shenyang Aerospace University, Shenyang, Liaoning 110136, China

Abstract: Based on the cylinder fluidized bed built by Shedin and Hassanto, a three-dimensional Euler–Euler simulation of the effect on the convective heat transfer characteristics between the fluidized particles and the inner heated surface was carried out under different operation conditions including particles sphericity, superficial gas velocity and initial solid packing height in the vertical fluidized bed. Moreover, the experimental average temperature had been chosen to test the validity of numerical average temperature. Contour plots of transient distribution of solid volume fraction and solid temperature have



been obtained in fluidized bed on horizontal cross-section in order to understand the effects of hydrodynamic and flow patterns on heat transfer characteristics. The results showed that the solid phase concentration distributed from the initial centrally symmetric annular stratification to the final severely turbulent fluidization by observing contour plots of the solid-phase volume fraction on horizontal cross-section. Solid temperature decreased from center to periphery in the radial direction at initial state since the gas–solid heat exchange rate affected the particle temperature in the entire bed. The temperature distribution of particles was non-uniform on the annular region due to the bed without being fluidized. With the process of fluidization underway, the particles temperature distribution tended to be uniform in horizontal cross-section because the bed material heat transferred from the center's cylindrical heater wall to the bed. The effective thermal conductivity was used to calculate the individual gas and solid phase convective heat transfer coefficient from heater surface to fluidized beds. Not only the average temperature of both heating wall and fluid but the difference of the average temperature between wall and fluid were decreasing with increasing superficial gas velocity. It enhanced turbulence intensity and led to increase the heat transfer coefficient between heater surface and fluid with the same time. The solid average convective heat transfer coefficient grew up with the initial height increasing of the bed material due to the contact area enlargement of particles and the heated surface in the fluidized bed.

Key words: fluidized bed; two-fluid model; heat transfer characteristics; two-phase flow; convective heat transfer coefficient

收稿: 2018-01-19, 修回: 2018-04-19, 网络发表: 2018-09-13, Received: 2018-01-19, Revised: 2018-04-19, Published online: 2018-09-13
基金项目: 国家重点基础研究发展计划资助项目(编号: 2011CB201506)
作者简介: 王力军(1963–), 男, 辽宁省开原市人, 博士, 副教授, 主要研究方向为燃烧流动模拟, E-mail: wanglijun@sau.edu.cn.

引用格式: 王力军, 段叔平, 徐凌峰, 等. 柱形流化床传热特性的数值模拟. 过程工程学报, 2019, 19(1): 110–117.

Wang L J, Duan S P, Xu L F, et al. Numerical simulation on heat transfer in a cylindrical fluidized bed (in Chinese). Chin. J. Process Eng., 2019, 19(1): 110–117, DOI: 10.12034/j.issn.1009-606X.218119.

柱形流化床传热特性的数值模拟

王力军*, 段叔平, 徐凌锋, 孙嘉君

沈阳航空航天大学能源与环境学院, 辽宁 沈阳 110136

摘 要: 对 Shedid 等搭建的圆柱体流化床采用欧拉-欧拉法进行三维数值模拟, 考察了颗粒球形度、表观进气速度和床料初始堆积高度对流化床内垂直加热壁面与流动床料之间对流传热特性的影响, 采用有效导热系数分别计算气相和固相的对流传热系数。结果表明, 随表观进气速度增大, 流化床内颗粒物料湍流运动加剧, 加热壁面平均温度和流体平均温度下降, 壁面流体间传热平均温度差减小, 壁面流体间对流传热系数增大; 随初始床料高度增加, 流化床内颗粒与加热壁面的接触面积增大, 导致固相平均对流传热系数增大。

关键词: 流化床; 双流体模型; 传热特性; 两相流; 对流传热系数

中图分类号: TK229.66

文献标识码: A

文章编号: 1009-606X(2019)01-0110-08

1 前言

目前流化床反应器已广泛应用于化工和工业生产中, 具有物料混合效率高、传热效率高、化学反应快等优点^[1]。计算流体动力学(CFD)在流态化领域得到了充分重视和应用, 成为了解流体力学和多相流流动机制^[2,3]的强大工具。经典经验模型和研究方法由于其局限性很难获得微观层次颗粒的运动特征^[4,5], CFD 只需较少的经验公式^[6,7]即可得到反应器内流场、温度场和浓度场等微观数据。目前基于颗粒动力学理论的欧拉-欧拉方法(双流体模型)已广泛用于流化床的传热数值模拟^[8-10]。双流体模型或颗粒流模型将气相和固相均视为连续相, 各相由单独的守恒方程(连续性方程、动量和能量方程)描述, 相间相互作用由相间耦合表征^[11]。

Gidaspow^[12]提出了经典的双流体模型, 将颗粒相粘度处理为无粘度模型和常粘度模型, 两种模型均能成功地描述流化床内气固两相流动行为。Leinaal 等^[13]应用双流体模型研究了密相流化床内不同形状颗粒物料流动的动力学特性, 提出了适用于不规则颗粒的气固相间曳力模型, 能很好预测实验尺度下的气固流态化特性。Behjat 等^[14]研究了颗粒的流动特性和气固流化床反应器内的传热特性, 获得了反应器内气固相的温度分布和传热系数。Schmidt 等^[15]采用对称流化床模型研究了鼓泡流化床内换热管束和炉内物料的传热, 合理解释了管束周围鼓泡的动力学特性。Armstrong 等^[16]发现对称的流化床难以很好地表征颗粒的复杂特征, 增加管数会导致床内中气泡破裂, 从而增加颗粒运动, 以更好地提高传热效率。

基于欧拉-欧拉方法, 本工作以 Shedid 等^[17]搭建的圆柱体流化床为研究对象, 对不同工况下的内部加热器与床料间的对流传热系数进行模拟, 并与实验数据对比。

通过将不同颗粒形状下的气固相间曳力模型函数加载到 Fluent 计算过程中, 为采用欧拉-欧拉双流体模型研究颗粒形状对流化床内传热特性的影响提供理论参考; 分析了竖直式加热管壁面与气固两相流之间的对流传热特性, 为工程应用提供参考。

2 数学模型

双流体模型(TFM)被广泛用于模拟稠密气固两相流在流化床中的流动和传热, 控制单元网格内气相和固相均视为连续相且具有各自独立的体积分数。模型中颗粒相间作用通过颗粒粘度耦合, 即基于颗粒流动动力学理论^[11]描述粒子的波动性和粒子间的碰撞。气固相间作用通过气固曳力耦合, 采用 Huilin-Gidaspow 曳力函数模型^[18](结合了 Wen-Yu^[19]和 Ergun^[20]的模型), 并针对不同形状的物料颗粒进行曳力修正^[22]以研究颗粒形状对传热的影响。双流体模型的控制方程和本构方程如下:

质量守恒方程(连续性方程):

$$\text{气相: } \frac{\partial}{\partial t}(\varepsilon_g \rho_g) + \nabla \cdot (\varepsilon_g \rho_g \vec{v}_g) = 0 \quad (1)$$

$$\text{固相: } \frac{\partial}{\partial t}(\varepsilon_s \rho_s) + \nabla \cdot (\varepsilon_s \rho_s \vec{v}_s) = 0 \quad (2)$$

单元体内气相和固相的体积分数之和:

$$\varepsilon_g + \varepsilon_s = 1 \quad (3)$$

动量守恒方程(N-S 方程):

$$\begin{aligned} \text{气相: } & \frac{\partial}{\partial t}(\varepsilon_g \rho_g \vec{v}_g) + \nabla \cdot (\varepsilon_g \rho_g \vec{v}_g \vec{v}_g) = \\ & -\varepsilon_g \nabla p + \nabla \cdot \bar{\tau} + \varepsilon_g \rho_g \vec{g} + K_{sg}(\vec{v}_s - \vec{v}_g) \end{aligned} \quad (4)$$

固相:

$$\frac{\partial}{\partial t}(\varepsilon_s \rho_s \vec{v}_s) + \nabla \cdot (\varepsilon_s \rho_s \vec{v}_s \vec{v}_s) = -\varepsilon_s \nabla p + \nabla p_s + \nabla \cdot \bar{\bar{\tau}}_s + \varepsilon_s \rho_s \vec{g} + K_{gs}(\vec{v}_g - \vec{v}_s) \quad (5)$$

能量守恒方程:

$$\frac{\partial(\varepsilon_s \rho_s \psi_s)}{\partial t} + \nabla \cdot (\varepsilon_s \rho_s \psi_s \vec{v}_s) = \nabla \cdot \varepsilon_s k_{s,\text{eff}} \nabla T_s - \varepsilon_s \frac{\partial p_s}{\partial t} + \bar{\tau}_s \cdot \nabla \vec{v}_s + S_s + h_{sg}(T_s - T_g) \quad (6)$$

$$\frac{\partial(\varepsilon_g \rho_g \psi_g)}{\partial t} + \nabla \cdot (\varepsilon_g \rho_g \psi_g \vec{v}_g) = \nabla \cdot \varepsilon_g k_{g,\text{eff}} \nabla T_g - \varepsilon_g \frac{\partial p_g}{\partial t} + \bar{\tau}_g \cdot \nabla \vec{v}_g + S_g + h_{gs}(T_g - T_s) \quad (7)$$

$$h_{gs} = h_{sg} \quad (8)$$

式中, 下标 g 和 s 分别表示气相和固相, t 为时间(s), ε 为局部体积分, v 为速度(m/s), ρ 为密度(kg/m³), p 为压力(Pa), g 为重力加速度(m/s²), K_{gs} 为气固动量传递系数[kg/(m³·s)], τ 为压力应变张量(N/m²), h_{gs} 和 h_{sg} 为气相和固相的传热系数[W/(m³·K)], ψ 为比焓(J/kg), $k_{g,\text{eff}}$ 和 $k_{s,\text{eff}}$ 分别为气相和固相的有效导热系数[W/(m·K)], T 为温度(°C), S 为热源相。

基于 Huilin-Gidaspow 曳力函数, 不同颗粒球形度下的曳力修正:

$$K_{sg} = (1 - \phi_{gs}) K_{\text{Wen-Yu-Ganser}} + \phi_{gs} K_{\text{Ergun}} \quad (9)$$

$$K_{\text{Wen-Yu-Ganser}} = \frac{3}{4} \frac{\varepsilon_s \varepsilon_g \rho_g (\vec{v}_g - \vec{v}_s)}{d_s} C_{d0} \varepsilon_g^{-2.7} \quad (10)$$

$$K_{\text{Ergun}} = \frac{180 \varepsilon_s^2 \mu_g}{\phi^2 d_s^2 \varepsilon_g} + \frac{2.0 \varepsilon_s \rho_g (\vec{v}_g - \vec{v}_s)}{\phi d_s} \quad (11)$$

$$\phi_{gs} = 0.5 + \frac{\arctan[180 \times 2.0(\varepsilon_s - \varepsilon_{\text{smf}})]}{\pi} \quad (12)$$

$$C_{d0} = \frac{24}{Re_s L_1} \left[1.0 + 0.1118 (Re_s L_1 L_2)^{0.6567} \right] + \frac{0.4305 L_2}{1 + 3305 / Re_s L_1 L_2} \quad (13)$$

$$L_1 = \left(\frac{d_n}{3d_v} + \frac{2\phi^{-0.5}}{3} \right)^{-1} - 2.25 \frac{d_v}{D} \quad (14)$$

$$L_2 = 10^{1.8148(-\lg)^{0.5743}} \quad (15)$$

$$Re_{s0} = \frac{\varepsilon_g \rho_g d_v |\vec{v}_s - \vec{v}_g|}{\mu_g} \quad (16)$$

式中, $K_{\text{Wen-Yu-Ganser}}$ 和 K_{Ergun} 分别为采用 Wen-Yu-Ganser 和 Ergun 方法获得的气固动量传递系数, d_s 为颗粒当量直径(m), d_v 为颗粒的体积当量直径(m), d_n 为垂直于颗粒运动方向颗粒投影面积的当量直径(m), D 为流化床的当量直径(m), ϕ 为颗粒球形度, ϕ 为正切逆函数, L_1 , L_2 分别为斯托克斯形状因子和牛顿形状因子, ε_{smf} 为固相临界体积分, C_{d0} 为曳力系数, μ 为动力粘度(Pa·s), Re_{s0} 为不同形状颗粒固相雷诺数, Re_s 为固相雷诺数。

鉴于实验过程中流化床内的工况温度约为 20~300 °C, 辐射传热部分(低于 600 °C)可忽略不计^[21], 本研究中颗粒物料和加热壁面之间的传热仅考虑气相和固相的对流传热, 计算公式如下:

$$h = h_s + h_g = \frac{q}{T_{w,\text{num},i} - T_{\text{bulk,num},i}} \quad (17)$$

$$h_s = \frac{q_s}{T_{w,\text{num},i} - T_{\text{bulk,num},i}} = \frac{\varepsilon_s k_{s,\text{eff}} \left| \frac{\partial T_s}{\partial n} \right|}{T_{w,\text{num},i} - T_{\text{bulk,num},i}} \quad (18)$$

$$h_g = \frac{q_g}{T_{w,\text{num},i} - T_{\text{bulk,num},i}} = \frac{\varepsilon_g k_{g,\text{eff}} \left| \frac{\partial T_g}{\partial n} \right|}{T_{w,\text{num},i} - T_{\text{bulk,num},i}} \quad (19)$$

$$T_{\text{bulk,num}} = \frac{1}{N} \sum_{i=1}^5 T_{\text{bulk,num},i} \quad (20)$$

$$T_{w,\text{num}} = \frac{1}{N} \sum_{i=1}^5 T_{w,\text{num},i} \quad (21)$$

$$t_{\text{bulk,exp}} = \frac{1}{N} \sum_{i=1}^5 t_{\text{bulk,exp},i} \quad (22)$$

$$T_{w,\text{exp}} = \frac{1}{N} \sum_{i=1}^5 T_{w,\text{exp},i} \quad (23)$$

$$h_{\text{num,avg}} = \frac{1}{N} \sum_{i=1}^5 h_{\text{num},i} \quad (24)$$

$$h_{\text{exp,avg}} = \frac{1}{N} \sum_{i=1}^5 h_{\text{exp},i} \quad (25)$$

$$\text{MSVF} = \frac{1}{N} \sum_{i=1}^{50} \varepsilon_{s,i} \quad (26)$$

$$\text{MHTC} = \frac{1}{N} \sum_{i=1}^{50} h_i \quad (27)$$

其中气相和固相与加热器壁面间的有效导热系数^[22,23]为

$$k_{g,\text{eff}} = \left(\frac{1 - \sqrt{\varepsilon_s}}{\varepsilon_g} \right) k_g \quad (28)$$

$$k_{s,eff} = \frac{1}{\sqrt{\varepsilon_s}} k_g [\omega A + (1 - \omega) \Gamma] \tag{29}$$

$$\Gamma = \frac{2}{1 - B/A} \left[\frac{A-1}{(1 - B/A)^2} \frac{B}{A} \ln\left(\frac{A}{B}\right) - \frac{B-1}{1 - B/A} - \frac{B+1}{2} \right] \tag{30}$$

$$A = k_s / k_g, \quad B = 1.25(\varepsilon_s / \varepsilon_g)^{10/9}, \quad \omega = 7.26e^{-3} \tag{31}$$

式中，下标 exp 和 num 分别表示实验值和模拟值，*i* 表示几何位置变量，具体位置如图 1 所示，*w* 和 bulk 分别表示加热器壁面和流体颗粒团，avg 表示平均值，*h_g* 和 *h_s* 分别为气相和固相对流传热系数[W/(m²·K)]，*q* 为对流传热量(W/m²)，*n* 为垂直于传热面的单位法向量，*k_g* 和 *k_s* 分别为气相和固相的导热系数[W/(m·K)]，*N* 为数据测点数，MSVF 和 MHTC 分别为固相平均体积分数和平均对流传热系数[W/(m²·K)]；*Γ*、*A*、*B* 和 *ω* 为计算有效导热系数时的修正系数。

3 数值模拟

以 Shedd 等^[17]搭建的圆柱体流化床为模拟对象，床体外圆柱直径 0.152 m，内圆柱加热器壁面直径 50.8 mm，床高 0.9 m，物理模型示意图如图 1 所示。用高岭土颗粒作为床料，采用底部均匀布风，采用 Ni–Cr/Ni–Al (K 型) 热电偶测量加热器表面温度和流体温度，测温点坐标如图 1 所示。用流体模拟软件 Fluent 15.0 对流化床进行三维数值模拟，采用结构网格，网格数为 37800

(36×21×50)，时间步长设为 0.001 s。为获得流体区域内流体力学和温度分布的精确解，采用 SIMPLE 算法建立压力与速度的耦合关系。位于床底的入口为速度入口，流化床顶部的边界条件为压力出口。将边界条件定为气固两相无滑移壁面条件，流化床内壁边界设为热流密度作为电阻式加热壁面，流化床外壁为绝热壁面，其边界类型设为热流密度为 0。模拟所用边界条件及其它物性参数见表 1。

表 1 模拟参数
Table 1 Simulation parameters

Parameter	Value
Air density, ρ_g /(kg/m ³)	1.225
Particle density, ρ_s /(kg/m ³)	2320
Superficial gas velocity, U_0 /(m/s)	0.12, 0.15, 0.18, 0.24, 0.30, 0.36
Particle diameter, d_p /mm	0.280, 0.550
Minimum fluidization velocity for $d_p=0.280$ mm, $U_{mf,280}$ /(m/s)	0.059
Minimum fluidization velocity for $d_p=0.550$ mm, $U_{mf,550}$ /(m/s)	0.210
Heat flux, q /(W/m ²)	1114
Initial solid packing heights, H /cm	25, 35, 45, 55
Restitution coefficient, e	0.9
Air viscosity, μ_g /(kg/ms)	0.012
Initial packing rate, β	0.55
Gas phase thermal conductivity, k_g /[W/(m·K)]	0.0252
Solid phase thermal conductivity, k_s /[W/(m·K)]	0.9
Gas phase specific heat at constant pressure, $C_{p,g}$ /[J/(kg·K)]	1005
Solid phase specific heat at constant pressure, $C_{p,s}$ /[J/(kg·K)]	865

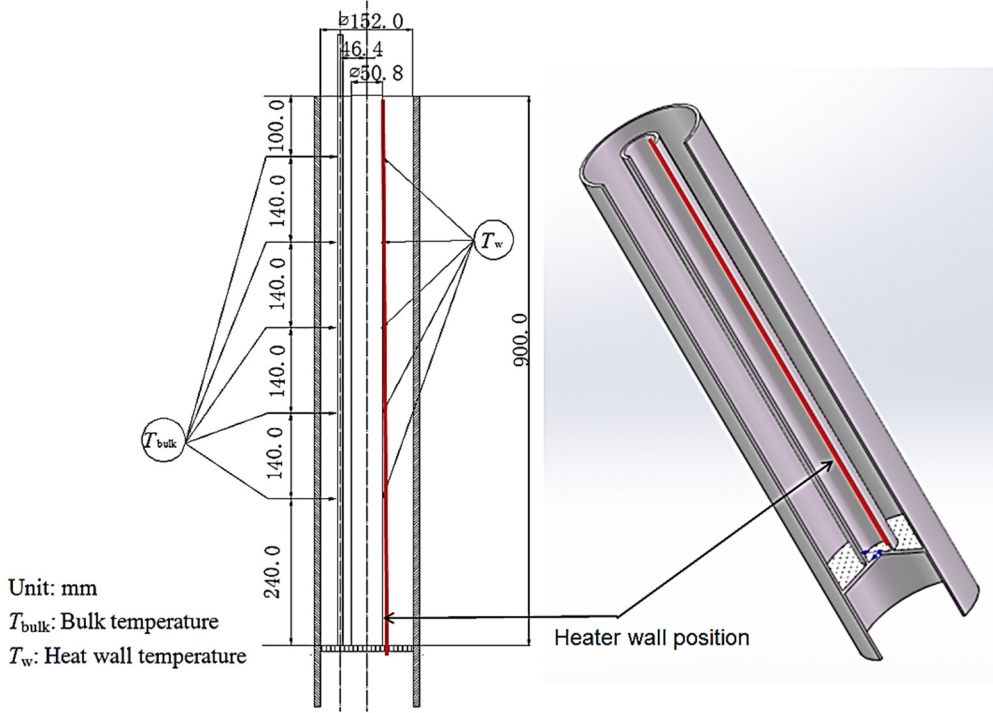


图 1 柱形流化床结构剖切示意图
Fig.1 The section view of the cylindrical fluidized bed structures

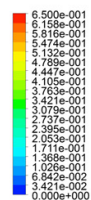
4 结果与讨论

4.1 流场与温度场分析及模型验证

不同模拟时刻横切面($z=0.45$ m)上的固相体积分数和颗粒温度分布云图见图2, 条件为床料初始高度 55 cm, 加热量 1114 W/m^2 , 进气表观速率 0.3 m/s , 球形颗粒粒

径 0.550 mm 。观察切面处的固相体积分数云图可发现流化床内颗粒物料从初始的静态环状分层到最终的剧烈湍动的流态化过程。虽然流化床的几何结构中心对称, 但伴随流态化进行, 气固相流场分布却为非中心对称。这是由于大量气泡从布风板底部持续上升变大, 上升过程中伴随物料颗粒剧烈的不规则湍流运动。

Solid volume fraction



Solid temperature/K

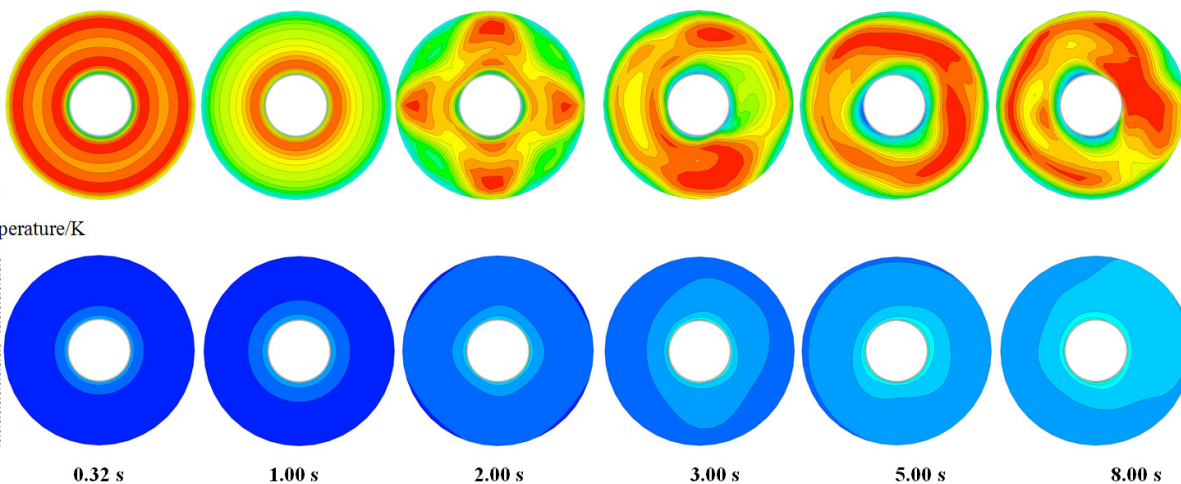
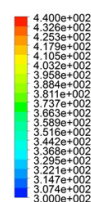


图2 不同时刻流化床横切面($z=0.45$ m)的固相颗粒体积分数分布云图和对应的温度云图

Fig.2 Contour plots of transient distribution of solid volume fraction and solid temperature in fluidized bed on horizontal cross-section of 0.45 m

0.32~1 s 时模拟的流场温度从中心加热壁面到外壁面沿径向递减, 这是由于流体颗粒团还未达到流态化。1~8 s 时, 随流体域内流体的流态化程度增强, 流动的气固两相流将热量持续地从中央加热表面运输到流体域中, 截面的平均温度逐渐升高。图3为流化床加热壁面和颗粒团平均温度模拟值和实验值随时间的变化。在床料初始高度 55 cm、加热量为 1114 W/m^2 , 球形颗粒粒径 0.280 mm 及表观进气速度 $U_0=0.12$ 和 0.36 m/s 的条件下, 10 s 时模拟的加热器壁面和流体颗粒团平均温度达到稳定, 与实验结果^[17]的相对误差小于 6.4%, 验证了双流体传热模型的可行性。

4.2 颗粒形状对平均温度和对流传热系数的影响

在流化床内球形颗粒物料与不规则形状颗粒的流动特性差异主要是因为二者具有不同的球形度, 所用 4 种形状的床料颗粒正四面体、正六面体、高和直径相等的圆柱体、球体的球形度分别为 0.671698, 0.806667, 0.874307 和 1。不同颗粒球形度下加热壁面和流体的平均温度及对流传热系数的变化如图4所示, 在初始高度 35 cm、加热量 1114 W/m^2 和表观进气速率 0.3 m/s 的条件下, 直径 0.550 和 0.280 mm 的床料颗粒与加热表面之间的对流传热系数的模拟值随颗粒球形度增加而

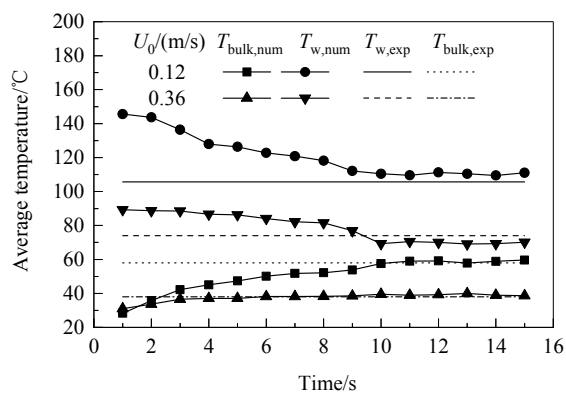


图3 不同时刻加热壁面和流体的平均温度的模拟值和实验值^[17]

Fig.3 Simulation and experimental^[17] results of wall and bulk average temperature at different numerical time

降低。这是由于空气掠过球形颗粒比掠过正四面体颗粒遇到的阻力小, 球形度小的不规则颗粒能从掠过的空气中获取更多动能, 湍流度比球形颗粒更高, 导致球形度低的不规则颗粒能从加热器表面带走更多热量, 比球形颗粒加热壁面温度低而流体颗粒团温度较高。从图4可看出, 小粒径颗粒(0.280 mm)加热表面和气固流体之间的温度差低于大粒径颗粒(0.550 mm), 且平均对流传热

系数($h_{\text{avg,num}}$)较高。这是因为小粒径颗粒比大粒径颗粒更易流态化,即临界流态化速度较低,在相同表观进气速度下流体域内的小粒径颗粒的湍流度更大,与加热器表面的碰撞频率较高,传热效果较强。

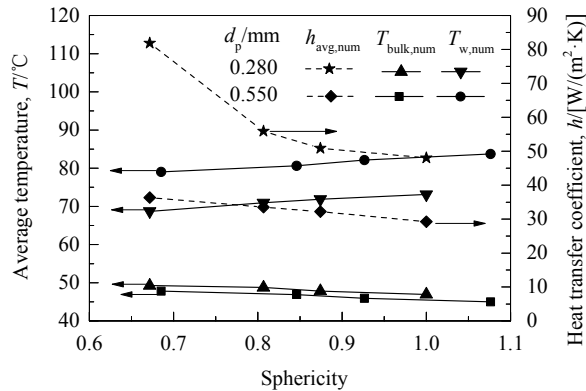


图 4 不同颗粒球形度下加热壁面和流体的平均温度及对流传热系数的变化

Fig.4 Variation of wall and bulk temperature and average convective heat transfer coefficient with different particle sphericity

4.3 表观速度对平均温度和对流传热系数的影响

不同表观速度下加热壁面平均温度和流体平均温度的实验值和模拟值的比较见图 5。由图可知,在初始高度 35 cm、加热量 1114 W/m^2 和球形颗粒直径 $d_p=0.280 \text{ mm}$ 条件下两个位置的平均温度均随表观进气速度增大而降低,模拟和实验值变化趋势一致,且在 $U_0=0.12 \text{ m/s}$ 时模拟的壁面温度较高。根据式(17)可知,相同热流密度下,壁面和流体的传热平均温度差越大,流体和加热壁面之间的对流传热系数越小。

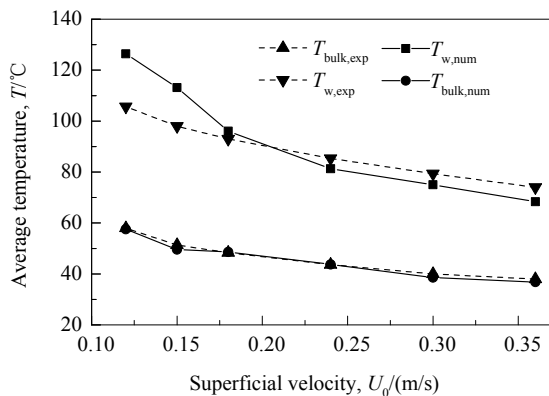


图 5 不同表观气速下加热壁面和流体的平均温度的变化
Fig.5 Variation of wall and bulk temperature against superficial gas velocity

不同表观进气速度下加热壁面和流体之间的平均对流传热系数如图 6 所示。由图可知,随表观速度增加,壁面和流体的平均温差减小,壁面和流体之间的对流传热系数增大。这是由于表观速度增大导致流化床内颗粒湍流运动加剧,使颗粒间的传热增强^[24]。

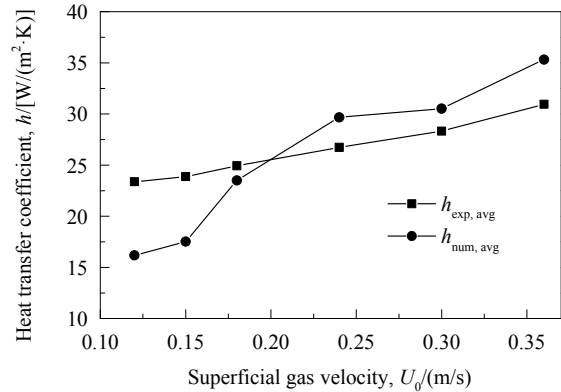


图 6 不同表观气速下加热壁面和流体之间的平均对流传热系数的变化

Fig.6 Variation of average convective heat transfer coefficient of wall and bulk against superficial gas velocity

4.4 床料高度对局部传热系数的影响

Olsson 等^[25]的研究表明,加热壁面处颗粒的更新频率和颗粒浓度对加热壁面和流体间的对流传热有重要影响。从式(18)可知,固相对流传热系数受固相体积分数的影响。图 7 是 $t=10 \text{ s}$ 时局部对流传热系数(h)、局部气相对流传热系数(h_g)、局部固相对流传热系数(h_s)和局部固相体积分数(ϵ_s)随床层高度的变化。由图可知,表观气速 $U_0=0.30 \text{ m/s}$ 、热流密度 $q=1114 \text{ W/m}^2$ 、球形颗粒直径 $d_p=0.280 \text{ mm}$ 的条件下,局部对流传热系数的波峰和波谷与固相体积分数趋于一致。在床层高度 $0.6\sim 0.9 \text{ m}$ 的位置固相体积分几乎为 0,流化床稀相区气相为主要的传热介质,该区域的气相对流传热系数明显大于固相。在密相区(加热器壁面位置 $0\sim 0.6 \text{ m}$),固相对流传热占主导。不同初始床料高度(H)下垂直加热表面处的平均对流传热系数和固相平均体积分数如图 8 所示, $H=25 \text{ cm}$ 时固相平均体积分数和平均对流传热系数分别为 0.065 和 $21 \text{ W/(K}\cdot\text{m}^2)$; $H=55 \text{ cm}$ 时固相平均体积分数和平均对流传热系数分别为 0.094 和 $27 \text{ W/(K}\cdot\text{m}^2)$ 。固相平均体积分数和平均对流传热系数随 H 增加而增大,流化床内颗粒与加热壁面的接触频率增加,导致固相平均对流传热系数增大。

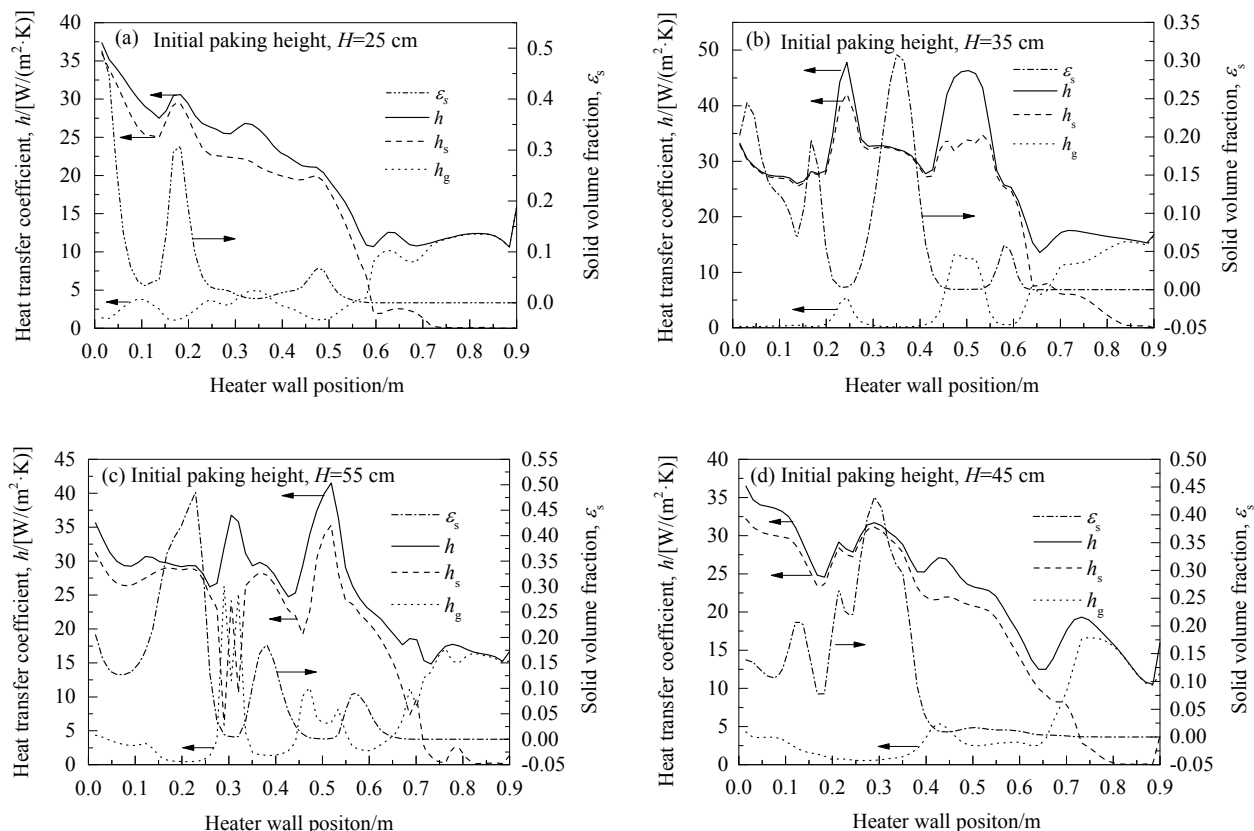


图7 加热壁面不同高度局部瞬态($t=10$ s)对流传热系数和固相体积分数的变化

Fig.7 Variation of local instantaneous heat transfer coefficients and solid volume fraction on the heater surface at the different heater wall positions at $t=10$ s

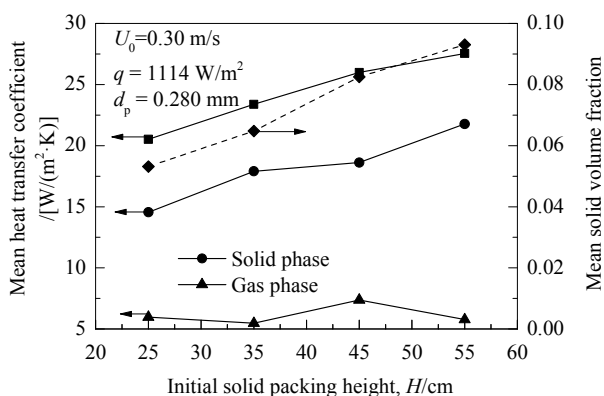


图8 不同初始床料高度下垂直加热表面处10 s内的平均对流传热系数和固相平均体积分数

Fig.8 Mean heat transfer coefficient and Mean solid volume fraction on the vertical heater surface at different initial solid packing heights in 10 s

5 结论

以 Shedid 等搭建的圆柱体流化床为研究对象,采用欧拉-欧拉法对流化床内垂直加热壁面与高岭土颗粒的对流传热特性进行三维数值模拟,考察了颗粒球形度、

表观进气速度和初始床料高度对物料和加热表面之间对流传热特性的影响,得到以下结论:

- (1) 流化床内床料颗粒与加热表面之间的对流传热效果随颗粒球形度增加而降低;小粒径颗粒比大粒径颗粒载热能力强,对流传热效果更好。
- (2) 表观速度增大导致流化床内颗粒湍流运动加剧,使颗粒间的传热增强。随表观速度增加,壁面和流体间的平均温差减小,对流传热系数增大。
- (3) 固相平均体积分数和平均对流传热系数随初始床料高度增加而增大,流化床内颗粒与加热壁面的接触频率增加,导致固相平均对流传热系数增大。
- (4) 在流化床的稀相区,气相是主要的传热介质,气相对流传热系数明显大于固相。在密相区固相对流传热占主导。

参考文献

- [1] Liu R, Jin B, Zhong Z, et al. Reduction of bed agglomeration in CFB combustion biomass with aluminum-contain bed material [J]. Process Safety and Environment Protection, 2007, 85(B5): 441-445.
- [2] Kalita P, Saha U K, Mahanta P. Parametric study on the hydrodynamics and heat transfer along the riser of a pressurized circulating fluidized bed unit [J]. Experimental Thermal and Fluid

- Science, 2013, 44(1): 620–630.
- [3] Dehnavi M A, Shahhosseini S, Hashemabadi S H, et al. CFD simulation of hydrodynamics and heat transfer in gas phase ethylene polymerization reactors [J]. *International Communications in Heat and Mass Transfer*, 2010, 37(4): 437–442.
- [4] Lim K S, Gururajan V S, Agarwal P K. Mixing of homogeneous solids in bubbling fluidized beds: theoretical modelling and experimental investigation using digital image analysis [J]. *Chemical Engineering Science*, 1993, 48(12): 2251–2265.
- [5] Gao J, Lan X, Fan Y, et al. Hydrodynamics of gas–solid fluidized bed of disparately sized binary particles [J]. *Chemical Engineering Science*, 2009, 64(20): 4302–4316.
- [6] Yusuf R, Halvorsen B, Melaaen M C. Eulerian–Eulerian simulation of heat transfer between a gas–solid fluidized bed and an immersed tube-bank with horizontal tubes [J]. *Chemical Engineering Science*, 2011, 66(8): 1550–1564.
- [7] Wang S Y, Liu G D, Wu Y B, et al. Numerical investigation of gas-to-particle cluster convective heat transfer in circulating fluidized beds [J]. *International Journal of Heat and Mass Transfer*, 2010, 53(15/16): 3102–3110.
- [8] Abdelmotalib H M, Ko D G, Im I T. A study on wall-to-bed heat transfer in a conical fluidized bed combustor [J]. *Applied Thermal Engineering*, 2016, 99(7): 928–937.
- [9] Armstrong L M, Gu S, Luo K H. Study of wall-to-bed heat transfer in a bubbling fluidised bed using the kinetic theory of granular flow [J]. *International Journal of Heat and Mass Transfer*, 2010, 53(21): 4949–4959.
- [10] Lu Y, Zhang T, Dong X. Bed to wall heat transfer in supercritical water fluidized bed: comparison with the gas–solid fluidized bed [J]. *Applied Thermal Engineering*, 2015, 88(2): 297–305.
- [11] Mostafazadeh M, Rahimzadeh M, Hamzei M. Numerical analysis of the mixing process in a gas–solid fluidized bed reactor [J]. *Powder Technology*, 2013, 239: 422–433.
- [12] Gidaspow D. Hydrodynamics of fluidization and heat transfer: supercomputer modeling [J]. *Applied Mechanics Reviews*, 1986, 39(1): 1–23.
- [13] Hua L N, Zhao H, Li J, et al. Eulerian–Eulerian simulation of irregular particles in dense gas–solid fluidized beds [J]. *Powder Technology*, 2015, 284: 299–311.
- [14] Behjat Y, Shahhosseini S, Hashemabadi S H. CFD modeling of hydrodynamic and heat transfer in fluidized bed reactors [J]. *International Communications in Heat and Mass Transfer*, 2008, 35(3): 357–368.
- [15] Schmidt A, Renz U. Eulerian computation of heat transfer in fluidized beds [J]. *Chemical Engineering Science*, 1999, 54(22): 5515–5522.
- [16] Armstrong L M, Gu S, Luo K H. The influence of multiple tubes on the tube-to-bed heat transfer in a fluidized bed [J]. *International Journal of Multiphase Flow*, 2010, 36(11/12): 916–929.
- [17] Shedid M H, Hassan M A M. Heat transfer characteristics of the fluidized bed through the annulus [J]. *Heat Mass Transfer*, 2016, 52(9): 1943–1952.
- [18] Gidaspow D, He Y, Lu H. Hydrodynamic modeling of binary mixture in a gas bubbling fluidized bed using the kinetic theory of granular flow [J]. *Chemical Engineering Science*, 2003, 58(7): 1197–1205.
- [19] Wen C Y, Yu Y H. *Mechanics of fluidization* [J]. *Chemical Engineering Progress Symposium Series*, 1966, 62(1): 100–111.
- [20] Ergun S. Fluid flow through packed columns [J]. *Chemical Engineering Progress*, 1952, 48(2): 89–94.
- [21] Natale F D, Lancia A, Nigro R. Surface-to-bed heat transfer in fluidised beds: effect of surface shape [J]. *Powder Technology*, 2007, 174(3): 75–81.
- [22] El-Beheri S M, El-Askary W A, Hamed M H, et al. Hydrodynamic and thermal fields analysis in gas–solid two-phase flow [J]. *International Journal of Heat and Fluid Flow*, 2011, 32(3): 740–754.
- [23] Kuipers J A M, Prins W, Van-Swaaij W P M. Numerical calculation of wall-to-bed heat transfer coefficients in gas-fluidized beds [J]. *AIChE Journal*, 1992, 38(7): 1079–1091.
- [24] Patil D J, Smit J, Van Sint Annaland M, et al. Wall-to-bed heat transfer in gas–solid bubbling fluidized bed [J]. *AIChE Journal*, 2006, 52(1): 58–74.
- [25] Olsson S E, Almstedt A E. Local instantaneous and time-averaged heat transfer in a pressurized fluidized bed with horizontal tubes: influence of pressure, fluidization velocity and tube-bank geometry [J]. *Chemical Engineering Science*, 1995, 50(20): 3231–3245.